Exploring the characteristics of a vehicle-based temperature dataset for kilometre-scale data assimilation

It is advisable to refer to the publisher's version if you intend to cite from the work. See Guidance on citing.

To link to this article DOI: http://dx.doi.org/10.1002/met.2058

www.reading.ac.uk/centaur

CentAUR

Central Archive at the University of Reading

Reading's research outputs online

RESEARCH ARTICLE

Exploring the characteristics of a vehicle-based temperature dataset for kilometre-scale data assimilation

Zackary Bell[1] [ID] | Sarah L. Dance[1,2] [ID] | Joanne A. Waller[3] [ID]

[1]Department of Meteorology, University of Reading, Reading, UK

[2]Department of Mathematics and Statistics, University of Reading, Reading, UK

[3]Met Office@Reading, University of Reading, Reading, UK

Correspondence
Zackary Bell, Department of Meteorology, University of Reading, Earley Gate, Whiteknights Road, Reading RG6 6ET, UK.
Email: z.n.bell@pgr.reading.ac.uk

Abstract

Crowdsourced vehicle-based observations have the potential to improve forecast skill in convection-permitting numerical weather prediction (NWP). The aim of this paper is to explore the characteristics of vehicle-based observations of air temperature in the context of data assimilation. We describe a novel low-precision vehicle-based observation dataset obtained from a Met Office proof-of-concept trial. In this trial, observations of air temperature were obtained from built-in vehicle air-temperature sensors, broadcast to an application on the participant's smartphone, and uploaded, with relevant metadata, to the Met Office servers. We discuss the instrument and representation uncertainties associated with vehicle-based observations and present a new quality-control procedure. It is shown that, for some observations, location metadata may be inaccurate due to unsuitable smartphone application settings. The characteristics of the data that passed quality control are examined through comparison with United Kingdom variable-resolution model data, roadside weather information station observations, and Met Office integrated data archive system observations. Our results show that the uncertainty associated with vehicle-based observation-minus-model comparisons is likely to be weather-dependent and possibly vehicle-dependent. Despite the low precision of the data, vehicle-based observations of air temperature could be a useful source of spatially-dense and temporally-frequent observations for NWP.

KEYWORDS

crowdsourced data, data assimilation, dataset of opportunity, km-scale numerical weather prediction, quality control, road-surface energy balance, vehicle-based observations

1 | INTRODUCTION

Convection-permitting numerical weather prediction (NWP) requires a large number of observations of high spatio-temporal resolution to constrain short-term forecasts (Sun et al., 2014; Gustafsson et al., 2018; Dance et al., 2019). However, due to the cost of installation, management, and maintenance of observing instrumentation, it may be impractical to extend traditional scientific observing networks to provide sufficient additional relevant observations. A potential alternative source of inexpensive observations is from opportunistic data generated by the public or other organizations (Blair et al., 2021; Waller, 2020).

The application of opportunistic datasets in NWP has been a popular area of research in recent years (Hintz et al., 2019a). Observations from personal weather stations (PWSs) (Chapman et al., 2017; Meier et al., 2017; Nipen et al., 2020; Steeneveld et al., 2011; Wolters & Brandsma, 2012) and smartphones (Droste et al., 2017; Hintz et al., 2020, 2021; Hintz 2019b; Madaus & Mass, 2017; Overeem et al., 2013) are commonly obtained through crowdsourcing. Such observations may be inaccurate when compared with traditional scientific observations. However, the number of crowdsourced observations available has the potential to far exceed the number of scientific surface observations currently produced (Muller et al., 2015). Opportunistic datasets can also be obtained from partnerships with other organizations. For example, roadside weather information station (RWIS) data obtained from highways agencies are currently assimilated into the Met Office United Kingdom variable-resolution (UKV) model (Gustafsson et al., 2018).

Observations obtained from vehicles are another dataset of opportunity (Mahoney III & O'Sullivan, 2013). Similarly to PWS and smartphone observations, vehicle-based observations can be obtained through crowdsourcing and will therefore be most densely distributed in urban areas and on major transport networks. Vehicle-based observations can also be obtained through several non-crowdsourcing methods. For example, the data can be obtained directly from vehicle manufacturers through connected vehicle initiatives (Mahoney III & O'Sullivan, 2013), from built-in sensors of vehicle fleets via the controller area network (Mercelis et al., 2020), or through externally mounted sensors (Anderson et al., 2012). In this paper, vehicle-based observations of air temperature are obtained from built-in vehicle sensors through on-board diagnostic (OBD) dongles. This method of data collection, which is described in Section 3, could be used for crowdsourcing vehicle-based observations.

Vehicle-based observations are currently used to improve road weather modelling (Hu et al., 2019) and forecasts to combat adverse road weather conditions on transportation networks (Siems-Anderson et al., 2019). Karsisto and Lovén (2019) showed that assimilation of vehicle-based observations into the Finnish Meteorological Institute's road weather model had the greatest forecast impact factor when RWISs were sparse. The use of vehicle-based observations in NWP is still in its infancy, but their use for nowcasting has been investigated by the German weather service (DWD) (Hintz et al., 2019a). Additionally, an observing simulation system experiment conducted by Siems-Anderson et al. (2020) showed a modest but appreciable impact from assimilating simulated vehicle-based observations.

Before opportunistic datasets can be assimilated, they must undergo thorough quality control (QC) and

the contributions to their observation uncertainty identified and investigated. Bell et al. (2015) attributed the total uncertainty of crowdsourced PWS observations to five sources: calibration issues, communication and software issues, inaccurate metadata, design flaws, and error due to unresolved scales. As a result of these issues, which also apply to other opportunistic datasets, the implementation of QC procedures can become substantially more difficult than the QC for traditional observations. In some studies, over half of the crowdsourced data were removed by the QC procedure (Meier et al., 2017; Madaus & Mass, 2017; Hintz et al., 2019b). Siems-Anderson et al. (2019) developed QC for vehicle-based observations from disparate sources for use in road weather forecasting systems. However, some of these QC tests required a large number of observations to be in close spatio-temporal proximity such that spatial comparisons can be used and were therefore not applicable to our dataset. A new QC procedure, described in Section 3.3, was developed for this dataset that used some existing and some novel QC tests.

Understanding the characteristics of opportunistic observations is key to their effective use in NWP (Waller, 2020). For data assimilation, an understanding of the instrument and representation errors that contribute to the total observation uncertainty is required. Important meteorological features such as sharp discontinuities caused by precipitation processes can be observed by opportunistic observations but will likely be misrepresented by an NWP model (Mahoney III & O'Sullivan, 2013). Hence, it is likely that there will be significant representation error caused by the mismatch in scales observed and modelled (Janjić et al., 2018). The instrument and representation components of the vehicle-based observation uncertainty are discussed in Section 2. For the vehicle-based observations of air temperature examined in this study, an important physical feature misrepresented by an NWP model will be the underlying road surface. The influence of roads on the air temperature measured by vehicles will be complex as the road-surface energy balance (RSEB) at a given location is substantially affected by the availability of water, the quantity of visible sky, and the amount of traffic (Anandakumar, 1999; Chapman & Thornes, 2011; Karsisto & Lovén, 2019; Oke et al., 2017). To properly understand the discrepancy between what is observed and modelled, it is necessary to examine the characteristics of the differences between the model and the observations. The objective of this paper is to explore the characteristics of a vehicle-based temperature dataset through comparison with other datasets.

The format of this paper is as follows. In Section 2, the uncertainties associated with vehicle-based observations of air temperature are discussed. The Met Office trial used to obtain the vehicle-based observations in this

BELL ET AL.

Meteorological Applications
Science and Technology for Weather and Climate
Open Access
RMetS

3 of 19

study, the datasets used for comparison, and the novel QC procedure applied to the vehicle-based observations are detailed in Section 3. The results of the new QC process highlight that the observation location metadata can be inaccurate due to poor global positioning system (GPS) signal and application settings. A comparison between vehicle-based observations and other datasets is given in Section 4. Our novel results show that the uncertainty of vehicle-based observations is likely weather-dependent and possibly vehicle-dependent. In Section 5 our results are summarized, and we conclude that vehicle-based observations are a promising opportunistic dataset for convection-permitting data assimilation.

2 | UNCERTAINTIES IN VEHICLE-BASED OBSERVATIONS OF AIR TEMPERATURE

2.1 | Vehicle-based observations of air temperature from built-in sensors

Most modern vehicles are equipped with a sensor to measure the air temperature of the surrounding atmosphere. Throughout this paper, these sensors will be referred to as external air-temperature sensors. Measurements obtained from external air-temperature sensors are used by vehicle air conditioning systems to adjust cabin-air temperature (Abdelhamid et al., 2014) and alert the driver to safety hazards such as the possible presence of ice on the roads (Padarthy & Heyns, 2019). External air-temperature sensors are commonly negative temperature coefficient thermistors (FierceElectronics, 2014). The location of external air-temperature sensors will vary with vehicle make and manufacturer. Common placements are usually in the airflow at the front of the vehicle, such as behind the grill near the bottom of the vehicle or in the wing mirror (Tchir, 2016). We note that most vehicles also have a sensor that measures the air temperature inside the vehicle engine, commonly referred to as the intake air-temperature sensor. These measurements, however, are contaminated with heat from the vehicle engine and hence will not be representative of the true atmospheric conditions.

2.2 | Instrument error

Built-in vehicle sensors are not intended to give high-quality meteorological information. As such, observations of air temperature from external air-temperature sensors are likely to have substantial instrument uncertainty. There are several sources of instrument uncertainty for vehicle-based observations of air temperature:

1. The observations may be affected by extraneous influences (Mahoney III & O'Sullivan, 2013).
2. The sensing instrument may not be as accurate or precise as required for meteorological applications (Mahoney III & O'Sullivan, 2013).
3. The ventilation of the sensing instrument may be inadequate (G. Harrison, 2015).

We now discuss these issues in more detail.

The extraneous influences that vehicle-based observations of air temperature are subject to include heating from the vehicle engine or the underlying road surface. The degree of vehicle influence on the observations will be determined by the sensors proximity to the vehicle engine. Mercelis et al. (2020) found that observations of air temperature from external air-temperature sensors situated far away from the vehicle engine were consistent with reliable observations obtained from road weather information stations. In contrast, observations obtained from sensors near the vehicle engine had to be discarded due to sensor biases. While external air-temperature sensor placement is usually chosen to mitigate the influence of engine heat (Tchir, 2016), radiation reflected from the road surface can be incident on the sensor. Observations of air temperature from external air-temperature sensors in such circumstances may be warmer than the true ambient conditions.

The precision of an observation will depend on the number of significant figures available for the digital representation of the measured value (the concept we have called precision is known in metrology as resolution (BIPM et al., 2012)). The difference between a continuous variable and its imprecise digital representation is known as the quantization error (Widrow et al., 1996). As the sensing instruments used for opportunistic datasets are not intended to give high-quality meteorological information, quantization uncertainty will likely be part of the instrument uncertainty (e.g., Mirza et al., 2016).

Adequate sensor ventilation is necessary to ensure accurate observations of air temperature (Harrison & Burt, 2020). Sensor ventilation for external air-temperature sensors is determined by how fast the vehicle is moving (e.g., Knight et al., 2010).

2.3 | Representation error

Representation error is defined as the difference between a perfect observation and a model's representation of that observation (Bell et al., 2020; Janjić et al., 2018). The model's representation of an observation is calculated using an observation operator. An observation operator is a function that maps the model state into observation

space. According to Janjić et al. (2018), the representation error consists of three components:

1. The pre-processing error caused by the incorrect preparation of an observation.
2. The observation operator error due to any incorrect or approximate observation operators used in the assimilation of an observation.
3. The error due to unresolved scales and processes when there is a mismatch in scales and processes observed and modelled.

We now discuss these errors in more detail.

The pre-processing error for vehicle-based observations of air temperature can be caused by the data collection and QC procedures. The height of external air-temperature sensors will vary with vehicle type and sensor-height metadata will likely be unavailable in the collection of crowdsourced datasets. Hence, the observations must be assigned a height that may differ from the true height resulting in a height assignment error. The QC for the vehicle-based observations is discussed in Section 3.3.

Since air temperature is usually an NWP variable, the observation operator for vehicle-based observations may be a simple interpolation operator. An observation operator error may result from the misrepresentation of the vehicle-based observation height by the NWP model. The resolution of NWP models is likely to be too coarse to represent the elevation of the vehicle-based observations properly (Waller et al., 2021). This mismatch in elevation between a surface observation and a NWP model field is normally accounted for by correcting the observation to be at the same height as the model field. As air temperature is expected to change with altitude in the surface layer (Stull, 1988a), the model height selected by the observation operator will influence the value of the model-equivalent observation.

For vehicle-based observations of air temperature, errors due to unresolved scales and processes are likely to be caused by deficiencies in the modelling of the local road-surface energy balance (RSEB). The RSEB describes the relationship between the net radiation into the road surface, the heating caused by traffic, the ground heat flux density, the sensible heat flux density, and the latent heat flux density (Karsisto & Lovén, 2019). The amount of radiation absorbed by the road will vary across the road due to the sky-view factor and traffic effects (Chapman & Thornes, 2011). The sky-view factor indicates the amount of shielding from radiative heating and cooling and may be highly spatially variable due to trees or buildings near the road. Chapman and Thornes (2011) showed a rural example where the sky-view factor caused road-surface temperature to vary by almost 3°C. Traffic effects include the generation of turbulence by vehicles, friction heat dissipation from tyres, sensible heat flux from vehicle engines, heat and moisture from exhaust fumes, and the blocking of incoming solar radiation and outgoing longwave radiation from the road surface (Chapman & Thornes, 2005; Prusa et al., 2002). Gustavsson et al. (2001) found that, during morning commuting hours in urban areas, traffic caused the road-surface temperature to increase by approximately 2°C.

The materials used for road surfaces have a large heat capacity such that much of the radiation absorbed by the surface is converted into ground heat flux (Anandakumar, 1999). The remaining turbulent heat fluxes are determined by the amount of water available at the road surface (Oke et al., 2017). If the road surface is dry, the remaining energy is entirely converted to sensible heat, which will result in a strong vertical air-temperature gradient near the road surface. Conversely, if water is available at the road surface, some of the remaining energy is converted into latent heat and the air-temperature profile near the surface will be more uniform.

A common approach for modelling surface fluxes in NWP is through tile schemes (Essery et al., 2003). Using this approach, the surface flux of a grid box is the weighted average of several different surface fluxes and hence may differ from the local RSEB substantially.

For road forecasting applications, outputs from NWP are post-processed in order to take better account of the road physics (e.g., Clark, 1998; Coulson et al., 2012). For this initial study, we do not use these post-processing techniques for simplicity. However, in principle, a more sophisticated observation operator could use a similar approach to road forecasting models and reduce the uncertainty due to unresolved scales.

3 | METHODOLOGY

3.1 | The Met Office trial

From February 20th 2018 to April 30th 2018 the Met Office ran a proof-of-concept trial to collect vehicle-based observations of air temperature from 31 volunteers. The measuring instruments used in this trial are those built-in by the manufacturer of the vehicle. In this trial, OBD dongles were used to broadcast reports from the vehicle engine management interface to an application (app) installed on a participant's smartphone via Bluetooth. Additional metadata derived from the smartphone were appended to the report, and uploaded to the Met Office Weather Observations Website (Kirk et al., 2021) using the smartphone's connection to the mobile network (3G, etc.). A complete description of this trial can be found in Bell et al. (2021). We now note some of the important aspects of the trial below.

The data collection frequency and GPS update period were set to 1 min, while the minimum distance for a GPS update was set to 500 m. We also note that a known fault that occurred during this trial was for engine-intake temperature (i.e., the air temperature inside the vehicle engine) to be recorded as air temperature for some observations. Observations were collected throughout the United Kingdom, with their locations corresponding to journeys undertaken by the participants.

The dataset obtained through this trial consists of 67,959 reports. Each report contains some combination of observations of air temperature, engine-intake temperature, and air pressure from built-in vehicle sensors. The observations of temperature have a precision of 1°C, while the observations of air pressure have a precision of 10hPa. We limit the scope of this study to air temperature only as engine-intake temperature will not reflect the true atmospheric-air temperature and air pressure has too low precision to be useful in NWP (World Meteorological Organization, 2021b). The metadata for each report includes vehicle speed (km/h), date-time (given by the application as date and 24-h clock time), GPS location, vehicle ID, and a unique observation ID. With the exception of vehicle speed, which was obtained by the OBD dongle, all metadata was derived by the smartphone app.

3.2 | Additional datasets used in this study

3.2.1 | Met Office integrated data archive system data

Met Office integrated data archive system (MIDAS) temperature data consist of observations of 1.5m-air temperature, which have a precision of 0.1°C and an uncertainty of 0.2°C for various locations in the United Kingdom (Met Office, 2006). We use MIDAS daily maximum and minimum temperature data in our QC procedure described in Section 3.3. We also use MIDAS hourly temperature data to provide a comparison with vehicle-based observations of air temperature that are within 1.5 km of a MIDAS station (see Section 4.2). These data are linearly interpolated to the time of a vehicle-based observation.

3.2.2 | NWP model data

To explore the characteristics of the vehicle-based observations that pass QC, we use Met Office 10-min UKV model data (Met Office, 2016). The UKV is a variable-resolution configuration of the Unified Model whose domain covers the United Kingdom and Ireland (Lean

et al., 2008). The inner domain has grid boxes of size 1.5 km × 1.5 km and fully covers the United Kingdom (Milan et al., 2020). Surrounding this is a variable-resolution grid with boxes whose edges steadily increase in zonal and/or meridional directions to 4 km in size.

In this study, we use 1.5m-air temperature and surface-air temperature defined as the air temperature at the boundary with the surface from short model forecasts known as the background (Milan et al., 2020). The UKV model data are interpolated to the time and horizontal location of a vehicle-based observation so that we can construct two observation-minus-background (OMB) datasets (i.e., one OMB dataset using surface-air data for the background and another OMB dataset using 1.5m-air temperature for the background). Since a vehicle-based observation and the horizontally interpolated background are both estimates of the true air temperature, their difference is equal to the difference of their errors. If their errors are independent, the variance of their differences will be equal to the sum of their individual error variances. Therefore, examining the statistics of the two OMB datasets will provide insight into the uncertainty of the vehicle-based observations. As the height of the external air-temperature sensor for each vehicle is unknown, we are unable to interpolate the model data to the height of a vehicle-based observation or correct the vehicle-based observation to be at the height of either UKV model field. It is likely that the vehicle-based observations are between the two model heights and are closer to the surface than the 1.5 m height.

The surface flux for each grid box is determined by expressing the percentage of land use as a combination of 5 vegetation and 4 non-vegetation tiles (Essery et al., 2003; Porson et al., 2010). For each grid box, the surface flux is obtained by calculating the sum of the weighted average of the fluxes from each tile (where instantaneous interaction between tiles is neglected). The UKV uses the urban canopy model MORUSES (Met Office-Reading Urban Surface Exchange Scheme) as the urban tile. MORUSES represents the impervious urban surface through a roof tile and a canyon tile (Hertwig et al., 2020). However, observations taken on motorways and major routes will often be surrounded by rural areas, and so the road fraction of the UKV grid box will be small. For example, a typical UK motorway traversing a rural grid box occupies less than 2% of the total area (Bremner, 2019).

3.2.3 | Roadside weather information station observations

Vehicle-based observations of air temperature from built-in sensors are known to be consistent with reliable

observations obtained from RWISs, provided the external air-temperature sensor is located away from the engine block (Mercelis et al., 2020). We therefore use RWIS data provided by Highways England (2018) to provide a comparison with similar point observations for different weather conditions. There are over 250 RWISs in England located along major roads and major routes providing various roadside meteorological information with a temporal frequency of 10 min (Buttell et al., 2020). In this study, we use RWIS observations of air temperature that have precision of at least 0.1°C. To give an indication of the total uncertainty of these observations, we note that the Met Office currently assimilates RWIS observations of air temperature into the UKV with an uncertainty of 1°C. We note that the height that RWISs measure air temperature is estimated to be between 2 and 3 m, but can be outside of this range if the site is located on a bank (Highways England, 2020). Road-state classifiers (i.e., dry, trace amounts of water, wet) provided by RWISs are used to indicate the availability of water at the road surface. The RWIS observations are linearly interpolated to the time that a vehicle passed a station.

3.3 | Quality control

In this section, we briefly describe the QC process applied to the vehicle-based dataset. Further details are given by Bell et al. (2021). We note that, due to the size and spatio-temporal sparsity of this dataset, we were unable to use spatial consistency QC tests.

Before the QC process was implemented, an initial filtering of the raw data from the trial was performed to ensure each observation had an air temperature observation and the relevant metadata needed for each test. This filtering removed 35,780 observations (52.6% of original dataset) due to either a missing air temperature observation or an invalid speed. The resultant dataset will be referred to as the filtered dataset.

The QC process applied to the vehicle-based dataset began with three tests applied in parallel: the climatological range test (CRT), the stuck instrument test (SIT), and the GPS test. Lastly, observations that passed each of these tests were then put through a sensor ventilation test (SVT). The final quality-controlled dataset (QC-dataset) consisted of all observations that passed the SVT. We now provide a brief description of each QC test.

The CRT checked if an observation was within a specified tolerance of a location-specific climatology. For this dataset, we used MIDAS daily temperature data (Met Office, 2006) to create monthly climatology datasets. These datasets were constructed by determining the maximum and minimum air temperature of each MIDAS

station active during February–April 2018 from pre-2018 data. The CRT was implemented by comparing the observation to the nearest (in terms of great circle distance) MIDAS station monthly climatology dataset. If the observation was within a 2°C tolerance of the climatological range of the MIDAS station, then the observation was passed. The 2°C tolerance was chosen as few observations were flagged by this test. However, larger tolerances may be more suitable for other vehicle-based datasets.

The SIT examined portions of vehicle-specific time-series to check whether the vehicle sensor was stuck on an air temperature value. This test required a vehicle identifier to determine observations that came from the same source (this may be unavailable in other crowdsourced observation studies due to data privacy concerns). The SIT was implemented by comparing an observation with all other observations from the same vehicle that occurred within a 15-min time window. If there was at least one observation that had a different value of air temperature to the tested observation, then the tested observation was passed. This test is essentially a simplified version of a persistence test (see Zahumenskỳ, 2004 for guidelines) that is able to account for any short journeys undertaken by participants during the trial and the low precision of the data.

The GPS test compared the location of an observation, denoted the test observation, relative to a prior observation from the same vehicle, denoted the reference observation, to evaluate the plausibility of the observation location metadata. The reference observation was at most 30 min before the test observation. As with the SIT, a vehicle identifier was required to determine if observations came from the same source. The GPS test was implemented by calculating the great circle distance between the test and reference observations, d_{test}. Then d_{test} was compared with the maximum and minimum distances estimated using the speed and time metadata for the vehicle. The maximum distance was estimated by

$$d^e_{\max} = \max(v_{\text{test}}, v_{\text{ref}}) \times \Delta t, \qquad (1)$$

where v_{test} and v_{ref} are the speeds of the test and reference observations, respectively, and Δt is the time-gap between the two observations. Similarly, the minimum distance was estimated by

$$d^e_{\min} = \min(v_{\text{test}}, v_{\text{ref}}) \times \Delta t. \qquad (2)$$

The test observation passed the GPS test provided $\Gamma_{\min} d^e_{\min} \leq d_{\text{test}} \leq \Gamma_{\max} d^e_{\max}$ where $\Gamma_{\min} = 0.6$ and $\Gamma_{\max} = 1.3$ are minimum and maximum multiplicative tolerance constants, respectively. For justification of the choice of $\Gamma_{\min}$ and $\Gamma_{\max}$, we refer the reader to Bell et al. (2021). Test observations with $\Delta t < 1$ min or $\max(v_{\text{test}}, v_{\text{ref}})$

BELL ET AL.

Meteorological Applications
Science and Technology for Weather and Climate
Open Access
RMetS

7 of 19

$< 25 \, \text{km/h}$ were passed if $d_{\text{test}} \leq \Gamma_{\max} d_{\max}^e$ as they were expected to be close to the reference observation (the specific choice of 25 km/h is related to the SVT discussed in the next paragraph). If a test observation did not have an observation from the same vehicle that occurred at most 30 min prior, then it was left unclassified by the GPS test and became the reference observation for the next test observation in the vehicle time-series.

The SVT was the final QC test that was applied to the observations that passed all previous tests. This test involved checking that the speed metadata for each observation were above a predetermined sensor ventilation threshold, v_{sensor}. Examining the speed-temperature pairs of the filtered dataset (not shown) revealed that the largest air temperatures (above 26°C) occurred for speeds below 25 km/h. We therefore set $v_{\text{sensor}} = 25 \, \text{km/h}$. An observation passed the SVT if it had speed greater than v_{sensor}. Hence, any observations that were passed by the GPS test with low speeds were flagged by the SVT.

The QC-dataset contains 17,425 observations (25.6% of original dataset). A summary of the results of each QC test is provided in Table 1. We note that the SIT and GPS test could not test every observation in the filtered dataset due to unavailable or unsuitable reference observations. The most discriminating test was the GPS test. The majority of observations flagged by the GPS test were likely the result of the 500 m update distance default setting on the app. We also note that the SVT was a fairly discriminating test.

The QC approach taken with this dataset relied upon range validity and time-series tests. For crowd-sourced observations, time-series tests may be unsuitable as instrument identification metadata may be unavailable due to data privacy concerns. This may be overcome with appropriate encryption techniques (Verheul et al., 2019) or by performing the QC locally on the sensing device (Hintz et al., 2019b). Furthermore, the use of spatial consistency QC tests, which do not require instrument identification, would be a suitable replacement for time-series-based tests provided

there is a sufficient density of observations in a given area (Nipen et al., 2020).

4 | EXAMINATION OF THE QC DATASET

In this section we, compare the QC-dataset with UKV model data, RWIS data, and MIDAS hourly data. Illustrative examples of the effect of sunny and rainy weather conditions on vehicle-based observations are presented in Section 4.1, analysis of OMB and observation-minus-observation (OMO) statistics are discussed in Section 4.2, and vehicle-specific OMB statistics are examined in Section 4.3. We use UKV model data as the background in the OMB datasets and MIDAS hourly data in the OMO dataset.

The effects of different meteorological factors are quantified through statistical analysis of OMB departures grouped by sunny, cloudy, and rainy weather conditions and season. The sunny dataset will consist of observations that occur between 09:00 and 17:00 on days with at least 6 sunshine hours and less than 2 mm of rainfall. Therefore, the observations are likely to be influenced by solar radiation incident on UK roads. The rainy dataset will consist of observations that occur between 09:00 and 17:00 on days with at least 5 mm of rainfall and less than 2 h of sunshine. The cloudy dataset will consist of observations that occur between 09:00 and 17:00 on days with less 2 h of sunshine and 2 mm rainfall. Here, and throughout the remainder of this manuscript, the time is given in UTC. To obtain the weather-specific sub-datasets, we used the Met Office daily weather summaries (Met Office, 2018). The seasons we consider are winter, defined as all data occurring between February 20th and March 20th 2018, and spring, defined as all data occurring between March 21st and April 30th 2018. We note that these seasons do not conform to the usual definitions of meteorological winter and spring, but have been chosen due to the period of the Met Office trial and

TABLE 1 Summary of the results from all QC tests. The observations untested by the stuck instrument test and GPS test are due to a lack of reference observations. The observations passed by the sensor ventilation test form the QC-dataset.

QC test	Number of tested observations	Number of passed observations	Number of flagged observations	Number of untested observations
Climatological range test	32,179	32,129	50	0
Stuck sensor test	32,179	30,124	2008	47
GPS test	32,179	20,162	11,181	836
Sensor ventilation test	19,094	17,425	1669	0

so that the winter and spring datasets each contain a similar number of observations.

4.1 | Case studies on the effect of sunny and rainy weather conditions on vehicle-based observations

We now show three time-series of vehicle-based observations of air temperature, 10-min UKV 1.5m-air-temperature, and surface-air-temperature model data, and RWIS observations of air temperature. The routes traversed in each time-series began and ended in suburban areas and were predominantly on major roads and major routes in rural areas, which occasionally crossed urban areas. The location of each time-series is shown in Figure 1. We denote the time-series shown in Figure 2 as S1, Figure 3 as S2, and Figure 4 as R1. S1 and S2 are illustrative examples of the effect of sunny weather and R1 is an illustrative example of the effect of rainy weather on vehicle-based observations of air temperature. We note that the same vehicle produced the observations in S1 and R1, but a different vehicle produced the observations in S2. We also note that the large data gaps in the three time-series are due to breaks in the journeys, and the two small data gaps in S2 are due to observations removed by the QC procedure.

For clarity, we will refer to the OMB data using 1.5m-air temperature for the background as aOMB and using surface-air temperature data for the background as sOMB. Furthermore, we denote the bias (mean) and standard deviation of an aOMB dataset as μ_a and σ_a, respectively and the bias (mean) and standard deviation of a sOMB dataset as μ_s and σ_s, respectively.

Figure 2 shows data from sunny weather conditions on March 25th 2018, including the time-series S1, UKV, and RWIS data. The OMB summary statistics for S1 are shown in Table 2. The sun rose at 06:52 and set at 18:22 on this day. The RWIS stations included in this time-series recorded a dry road-state when the vehicle passed the station. As a result of these conditions, we expect the sensible heat flux emitted by the road to be large and the road surface to have a noticeable heating effect on the air temperature above (see Section 2.3). Additionally, we expect the surface-air temperature to be larger than the 1.5m-air temperature as the sensible heat flux emitted by the UKV surface will also be large. The mean difference between the interpolated RWIS observations and the nearest-in-time UKV model data reveals that RWIS observations are in most agreement with 1.5m-air temperature and in least agreement with surface-air temperature. There is a clear separation between UKV 1.5m-air temperature and surface-air temperature at the start of the time-series that gradually decreases as the net

FIGURE 1 Map of the United Kingdom showing the location of the three time-series discussed in Section 4.1. The red squares show the location of cities passed by or near to the routes travelled in the three time-series. The black diamonds show the location of the roadside weather information station stations passed on each journey. The two orange lines correspond to the sunny weather time-series and the blue line corresponds to the rainy weather time-series. The time-series S1 began near Exeter and travelled north towards Manchester. The time-series R1 travelled the same initial route as S1, but headed east from Birmingham towards Cambridge. The time-series S2 began in Edinburgh and travelled along the coast to Newcastle-upon-Tyne and then the vehicle travelled further inland and south towards Nottingham.

radiation absorbed by the UKV surface decreases. The vehicle-based observations generally lie between the model fields as seen by the difference in sign between the biases. The vehicle-based observations on average agree most with surface-air temperature as $|\mu_s| < |\mu_a|$. This is consistent with the height of the vehicle sensor, which is likely to be between the model field heights of 0 and 1.5 m but closer to 0 m than 1.5 m. Calculating the standard deviation of the sOMB and aOMB departures shows that the sOMB departures are more variable as $\sigma_a < \sigma_s$. We hypothesize that the variability of the UKV sensible heat flux induced by the sunny weather conditions is the mechanism responsible for the larger sOMB variability.
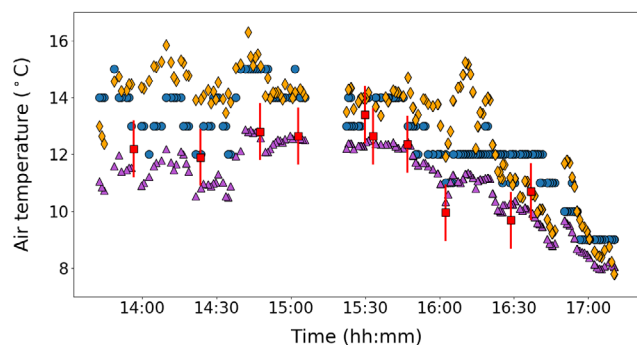
FIGURE 2 Time-series S1 of 212 vehicle-based observations of air temperature (blue circles) from a single vehicle driving along the M5 motorway on March 25th 2018 during sunny weather. Also shown are UKV 1.5m-air temperature (purple triangles) and UKV surface-air temperature (orange diamonds) linearly interpolated to the time and horizontal location of the vehicle-based observations, and RWIS observations of air temperature (red squares) linearly interpolated to the time the vehicle passed a station. The 1°C RWIS error bar represents the uncertainty used to assimilate RWIS observations into the UKV.
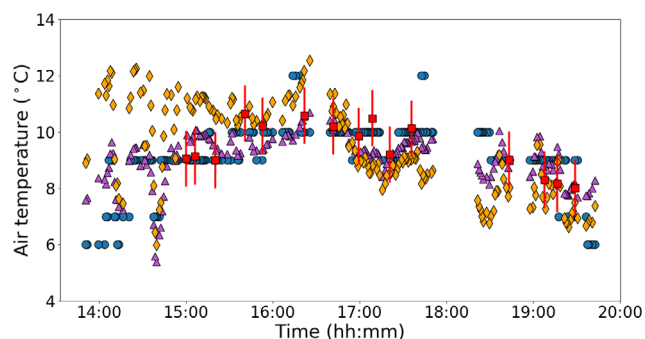

FIGURE 4 Time-series R1 of 259 vehicle-based observations of air temperature (blue circles) from a single vehicle driving along the M5 and M42 motorways and the A5 on March 30th 2018 during rainy weather conditions. Also shown are UKV 1.5m-air temperature (purple triangles) and UKV surface-air temperature (orange diamonds) interpolated to the time and horizontal location of the vehicle-based observations and RWIS observations of air temperature (red squares) interpolated to the time the vehicle passed a station. The 1°C RWIS error bar represents the uncertainty used to assimilate RWIS observations into the UKV.

FIGURE 3 Time-series S2 of 193 vehicle-based observations of air temperature (blue circles) from a single vehicle driving along the A1 and the M1 motorway on April 5th 2018 during sunny weather. Also shown are UKV 1.5m-air temperature (purple triangles) and UKV surface-air temperature (orange diamonds) interpolated to the time and horizontal location of the vehicle-based observations, and RWIS observations of air temperature (red squares) interpolated to the time the vehicle passed a station. The 1°C RWIS error bar represents the uncertainty used to assimilate RWIS observations into the UKV.

TABLE 2 Summary of the observation-minus-background statistics for the three time-series shown in Figure 1 using UKV 1.5m-air temperature and surface-air temperature as the background. The uncertainty in the mean for each time-series is less than 0.1°C.

Summary statistics	Time-series		
	S1	S2	R1
Number of observations	212	193	259
μ_a (°C)	1.4	0	0.7
σ_a (°C)	0.7	0.9	0.7
μ_s (°C)	−0.5	−0.3	0.4
σ_s (°C)	1.2	1.7	0.6

Figure 3 shows data from sunny weather conditions on April 5th 2018, including the time-series S2, UKV, and RWIS data. The OMB summary statistics for S2 are shown in Table 2. The sun rose at 05:27 and set at 18:40 on this day. The RWISs included in this time-series recorded a dry road-state when the vehicle passed the station. Similarly to the data in Figure 2, the RWIS observations are in most agreement with the UKV 1.5m-air temperature and in least agreement with surface-air
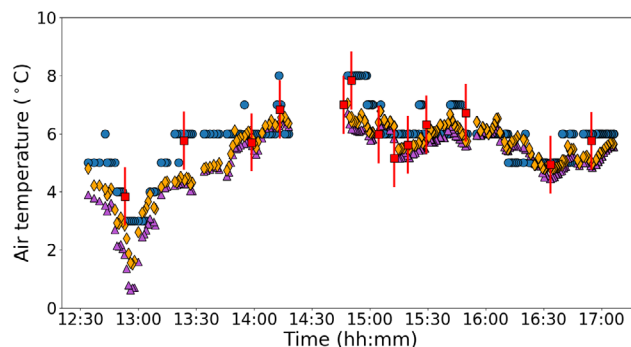
temperature. The surface-air temperature is larger than the 1.5m-air temperature for the first half of this time-series. From approximately 17:00 we see that 1.5m-air temperature is greater than surface-air temperature. We hypothesize that this is due to the stabilization of the boundary layer (Stull, 1988b). In contrast to S1, the vehicle-based observations are closest to UKV 1.5m-air temperature at the beginning of the time-series even though the sensible heat flux emitted from the road surface is expected to be greatest during this period. Possible reasons for this include cool breezes from the North Sea influencing the vehicle-based observations during the beginning of the time-series (see route map in Figure 1) or because the air temperature is measured by a different

vehicle's instrument. Furthermore, the difference between the biases μ_a and μ_s is large for S1 and small for S2. This, however, is likely due to the large number of observations that occurred during the evening for S2 when the temperature gradient between the surface and 1.5 m is expected to be small. Considering the observations from the first 3 h of S2 only, when the net solar radiation absorbed by the road and UKV surface is expected to be large, we find that the difference between the biases μ_a and μ_s is more profound. We note that the standard deviations σ_a and σ_s are larger for S2 than S1. This is likely due to the following two reasons. The first reason is the relatively long temporal length of the S2 time-series. The second reason is the possible transition to the nocturnal boundary layer as the surface layer starts to become stably stratified. However, it is also plausible that the placement of the external air-temperature sensors on the two vehicles is contributing to this behaviour.

Figure 4 shows data from rainy weather conditions on March 30th 2018, including the time-series R1, UKV, and RWIS data. The OMB summary statistics for R1 are shown in Table 2. The RWIS stations included in this time-series recorded either a wet road-state or trace amounts of water at the road surface when the vehicle passed the station. As a result of these conditions, we expect the sensible heat emitted by the road to be small and the road surface to have a reduced effect on the air temperature above (see Section 2.3). We note that the drop in air temperature between 12:30 and 13:30 is caused by an increase in altitude and an occluded front. The mean difference between the interpolated RWIS observations and the nearest-in-time UKV data reveals that RWIS observations are now in greater agreement with surface-air temperature than 1.5m-air temperature. The two UKV model fields are similar throughout the time-series with multiple segments where the vehicle-based observations are greater than both fields. The vehicle-based observations are on average greater than the UKV model data as the biases μ_a, $\mu_s > 0°C$ but agree more with surface-air temperature as $\mu_a > \mu_s$. This indicates that there are additional factors affecting the vehicle-based observations. Potential explanations for this behaviour are given in Section 4.2.4. We note that while the aOMB departures are more variable than the sOMB departures (i.e., $\sigma_a > \sigma_s$), they are similar in size.

We hypothesize that the effect of the sensible heat emitted by the road and UKV surfaces can be observed through comparison of the S1 and R1 time-series shown in Figures 2 and 4, respectively. In sunny weather, the sensible heat emitted by the road and UKV surface will be large, resulting in a stronger vertical air-temperature gradient between the surface and the 1.5 m height. In rainy weather, the sensible heat emitted by the road and UKV surface will be small, leading to a vertical air-temperature profile that is more uniform. This suggests that the difference between the biases μ_a and μ_s will be larger in sunny weather conditions than rainy weather conditions. The OMB standard deviations calculated for each time-series show a negligible difference for σ_a and a noticeable difference for σ_s between the two time-series. For the sOMB standard deviation σ_s, we see that it is smaller for rainy weather and larger for sunny weather. A possible reason for this is that the variability of the sensible heat emitted by the UKV surface will be greater in sunny weather than rainy weather. However, there may be other contributing factors such as the difference in observation operator error between the two time-series.

4.2 | Statistical analysis of observation-minus-background and observation-minus-observation departures

In this section, we investigate the uncertainty present in the QC-dataset through statistical analysis of OMB and OMO departures. The OMB datasets will be partitioned into weather-specific and seasonal sub-datasets so that we may examine how the OMB uncertainty changes with weather conditions and season. As there are only 347 observations within 1.5 km of a MIDAS station, we will not split the OMO dataset into weather-specific and seasonal sub-datasets. We now discuss the characteristics of each dataset.

4.2.1 | QC-dataset OMB and OMO statistics

The OMB and OMO statistics and the number of datapoints corresponding to the QC-dataset are given in Table 3. Examining the OMB statistics shows that the vehicle-based observations are in poorer agreement with 1.5m-air temperature than surface-air temperature as the biases satisfy $|\mu_a| = 0.7°C > |\mu_s| = 0.1°C$. This is expected as external air-temperature sensors likely measure air temperature nearer to the surface than to a height of 1.5 m. As $\mu_a = 0.7°C > 0°C$ and $\mu_s = 0.1°C > 0°C$, vehicle-based observations are on average warmer than both UKV model fields despite measuring the air temperature between them. Possible reasons for this behaviour are discussed in Section 4.2.4. For the standard deviations, we have that $\sigma_a = 1.2°C < \sigma_s = 1.6°C$, showing that the sOMB dataset is more variable than the aOMB dataset. This is also visible in the aOMB and sOMB distributions shown by the histograms in Figure 5a. While the distributions overlap substantially, a higher peak is seen for the aOMB distribution, whereas

TABLE 3 Summary of the OMB and OMO departure statistics for each dataset. The uncertainty in the mean for each dataset is less than 0.1°C.

OMB and OMO statistics				
Dataset	Number of observations	Departure	Mean (°C)	SD (°C)
QC-dataset	17,425	aOMB	0.7	1.2
		sOMB	0.1	1.6
	347	OMO	0.3	1.0
Sunny	1878	aOMB	1.1	1.2
		sOMB	−0.8	1.9
Cloudy	2366	aOMB	0.8	1.4
		sOMB	−0.1	1.7
Rainy	840	aOMB	0.6	1.0
		sOMB	0.3	1.0
Winter	7798	aOMB	0.5	1.3
		sOMB	0.3	1.6
Spring	9627	aOMB	0.8	1.2
		sOMB	0	1.6

the sOMB distribution has a larger left tail. It is likely that the background uncertainty of surface-air temperature is greater than 1.5m-air temperature due to the simplifying assumptions made by the UKV in modelling the SEB of a grid box (see Section 3.2.2).

Examining the OMO statistics reveals that vehicle-based observations are on average warmer than MIDAS observations. Comparing the OMO departure bias, $\mu_m = 0.3°C$, with the biases $\mu_a = 0.7°C$ and $\mu_s = 0.1°C$ obtained from the QC-dataset OMB departures, we find that $\mu_s < \mu_m < \mu_a$. Hence, the vehicle-based observations on average agree more with MIDAS data than 1.5m-air temperature but still agree most with surface-air temperature. While it is plausible that vehicle-based observations will generally agree more with MIDAS data than the UKV 1.5m-air temperature model data, we note the following two issues with these calculations. Firstly, the MIDAS data were not interpolated to the location of the vehicle-based observations and there will likely be differences in elevation between the two. As air temperature is expected to change with elevation in the surface layer (Stull, 1988a), the omission of any vertical interpolation may cause a bias. Secondly, while the variability of the OMO dataset is less than the variability of any OMB dataset shown in Table 3, it is calculated with far fewer observations making the statistic less reliable.

4.2.2 | Weather-specific OMB datasets

The OMB statistics and the number of datapoints for each weather-specific dataset are given in Table 3. For all weather types, the bias μ_a is positive, showing that vehicle-based observations are on average warmer than UKV 1.5m-air temperature regardless of weather conditions.

For the sunny and cloudy datasets, the bias μ_s is negative, whereas for the rainy dataset μ_s is positive. This agrees with the results of the three time-series discussed in Section 4.1. This also suggests that the vehicle-based observations studied in this paper may be colder on average than UKV surface-air temperature in dry conditions. The smallest differences between the biases occur for the rainy dataset ($\mu_a = 0.6°C$ and $\mu_s = 0.3°C$), while the largest difference occurs for the sunny dataset ($\mu_a = 1.1°C$ and $\mu_s = −0.8°C$), which is also seen in the S1 and R1 time-series discussed in Section 4.1. For the rainy dataset biases, we have that $\mu_a = 0.6°C > 0°C$ and $\mu_s = 0.3°C > 0°C$, which indicates the vehicle-based observations are on average warmer than the two UKV model fields. This suggests that there are other influencing factors on the vehicle-based observations that are not represented in the UKV as vehicles measure the air temperature between these two heights. Potential explanations for this behaviour are discussed in Section 4.2.4.

Inspection of the weather-specific standard deviations reveals that, for sunny ($\sigma_a = 1.2°C$ and $\sigma_s = 1.9°C$) and cloudy ($\sigma_a = 1.4°C$ and $\sigma_s = 1.7°C$) weather conditions, the sOMB dataset is noticeably more variable than the aOMB dataset. This difference in variability is shown in the histograms for the sunny dataset (Figure 5b) and the cloudy dataset (Figure 5c). The sunny aOMB distribution is unimodal and the sunny sOMB distribution is bimodal. The bimodal structure may be due to intermittent cloud cover on the days with less sunshine hours or the relatively
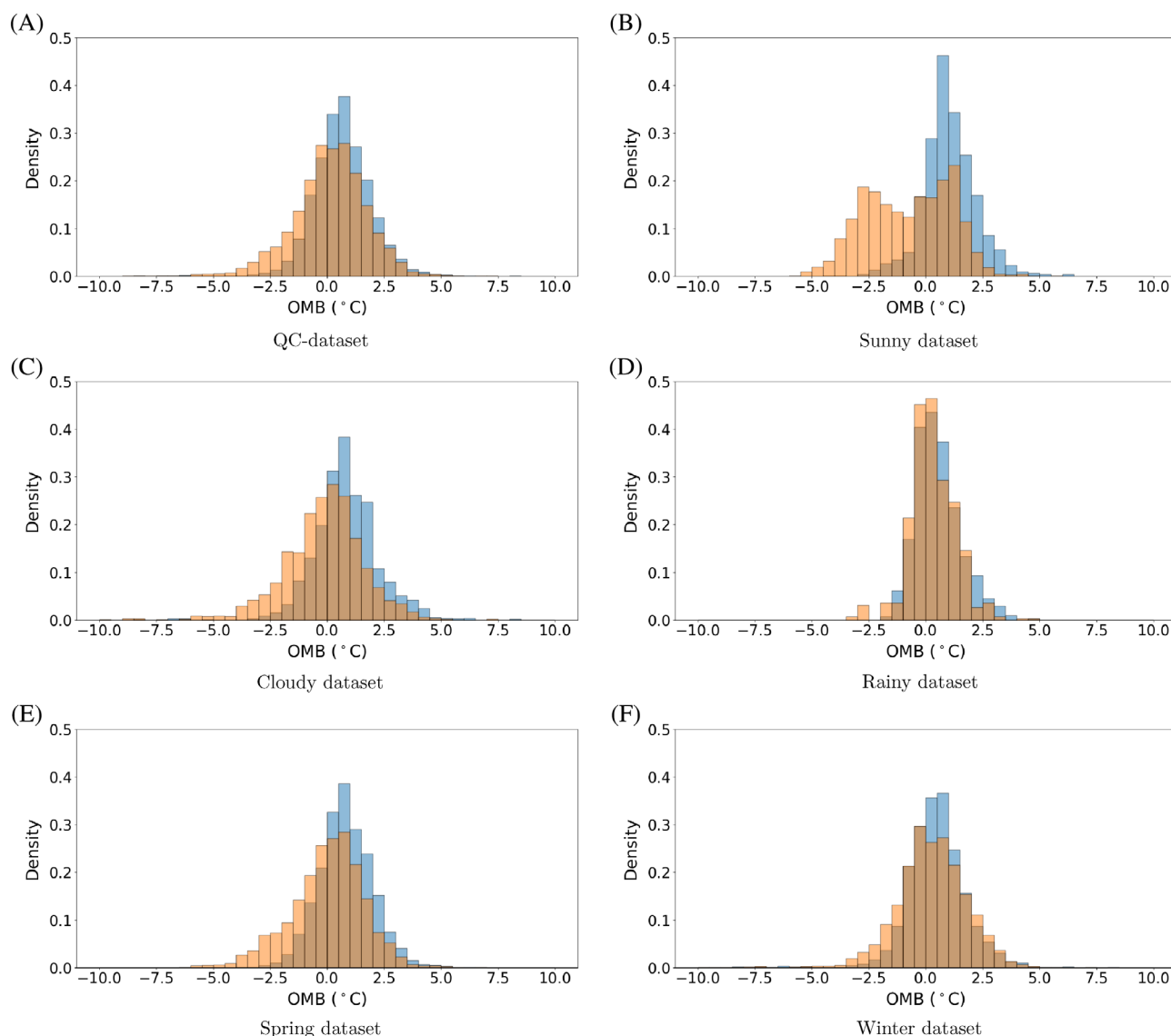
FIGURE 5 OMB histograms datasets corresponding to the datasets in Table 3. Bins of width 0.5°C have been used for each histogram. The blue bars correspond to the aOMB bins and the orange bars correspond to the sOMB bins.

small size of the sunny dataset. Similarly to the QC-dataset, the cloudy aOMB and sOMB distributions overlap substantially, but a higher peak is seen for the aOMB distribution and a larger left tail is seen for the sOMB distribution. For rainy weather conditions, the standard deviations $\sigma_a = 1.0°C$ and $\sigma_s = 1.0°C$ are equal to one decimal place leading to similar aOMB and sOMB distributions as shown in Figure 5d.

Overall, the variability for the weather-specific datasets agrees with the variability calculated for the time-series discussed in Section 4.1. We also find that the standard deviation is larger for the sunny sOMB dataset ($\sigma_s = 1.9°C$) than for the cloudy sOMB dataset ($\sigma_s = 1.7°C$). This behaviour is likely the result of the increased variability of the sensible heat emitted by roads and the UKV surface during sunny weather conditions due to the larger amount of solar

radiation absorbed by the two surfaces. This also suggests that the uncertainty of vehicle-based observations may be greatest in sunny weather conditions due to the combination of the radiative effects on the vehicle sensor and the representation uncertainty. Conversely, the aOMB standard deviation is largest for the cloudy dataset ($\sigma_a = 1.4°C$) and not the sunny dataset ($\sigma_a = 1.2°C$). This, however, may be due to changes in the sky-view factor due to variable cloud cover or because the cloudy dataset has more observations than the sunny dataset. We hypothesize that the rainy dataset standard deviations $\sigma_a = 1.0°C$ and $\sigma_s = 1.0°C$ are similar for the following three reasons. Rain increases the availability of water at the UKV surface, which reduces the emitted sensible heat flux, and hence the vertical air-temperature profile will be more uniform. There is also little to no sun at the times and locations of the vehicle-based

observations in the rainy dataset resulting in negligible radiation reflected by the road surface incident on the vehicle temperature sensor. Finally, the rainy dataset is the smallest of our three weather-specific datasets and so the OMB statistics are the least robust.

4.2.3 | Seasonal OMB datasets

The OMB statistics and the number of datapoints for the seasonal datasets are given in Table 3 and the histograms are plotted in Figures 5e (spring) and f (winter). We include information on the seasonal datasets to provide a baseline for the vehicle-specific analysis in Section 4.3. For the seasonal datasets, the vehicle-based observations are on average greater than the UKV model fields except for surface-air temperature in spring where they are approximately the same. Comparing the biases of the seasonal datasets, we see that the sOMB bias is smaller and the aOMB bias is greater in spring ($\mu_s = 0°C$ and $\mu_a = 0.8°C$) than in winter ($\mu_s = 0°C$ and $\mu_a = 0.8°C$). Inspection of the standard deviations of the seasonal datasets reveals that the sOMB variability is larger than the aOMB variability in both winter ($\sigma_s = 1.6°C$ and $\sigma_a = 1.3°C$) and spring ($\sigma_s = 1.6°C$ and $\sigma_a = 1.2°C$).

4.2.4 | Discussion of the uncertainty exhibited by the OMB datasets

In this section, we discuss several possible contributions to the uncertainty exhibited in the OMB statistics shown in Table 3.

- The vehicle-based observations of air temperature are precise to 1°C. The details of the observation processing by the OBD system and app are unknown. However, an indication of the expected size of the processing errors can be obtained by considering the quantization error from a typical procedure that rounds to the nearest integer. In this case, the root-mean-squared quantization error is $\sqrt{1/12}$ °C and may be a positive or negative error (Widrow et al., 1996).
- As discussed in Section 2.2, the external air-temperature sensors may exhibit a warm bias from extraneous sources. For instance, the sensor may be in close proximity to the vehicle engine or the location of the sensor may be inadequate for sensor ventilation. A rough estimate of the bias due to the vicinity of the engine is 5–25°C (Mercelis et al., 2021). However, there are several other factors that may be influencing this estimate (e.g., differing vehicles).

- In many makes and models of vehicle with on-board temperature sensors, there is an algorithm that delays the change of air temperature to avoid flickering or quick changes on the display for the driver. If the air temperature is obtained after the algorithm is applied, this could cause an issue in areas with strong temperature gradients.
- In unstable atmospheric conditions, the vertical air-temperature gradient between the surface and the 1.5 m height will be negative. When the sensible heat emitted by the road and UKV surfaces is large, the vertical air-temperature gradient will be large. Therefore, surface-air temperature will be warmer on average than vehicle-based observations, which likely measure air temperature between 20 and 100 cm above the road surface. Similarly, 1.5m-air temperature will be cooler on average than vehicle-based observations.
- The vehicle-based observations have not been corrected to the elevation of the model grid box. In NWP, it is common to correct surface observations using a standard adiabatic lapse rate of 0.0065°C/m (Cosgrove et al., 2003; Dutra et al., 2020).
- The UKV simulation of the diurnal cycle is not perfect and may contribute to the OMB uncertainty. For example, Boutle et al. (2016) studied a number of fog cases where the diurnal temperature range was underestimated by the UKV. However, since then, the UKV surface scheme has been updated. Warren et al. (2018) studied the new scheme by comparing model forecasts to observations in urban areas. The new scheme is much improved. In particular, it has better timing for the morning transition and better vertical mixing.
- The road-surface temperature is highly variable due to sky-view factors and traffic (Chapman & Thornes, 2011). As noted in Section 2.3, these factors can change the local temperature by as much as 2°C or 3°C.
- The difference in sensible heat emitted by the road surface and the UKV surface may contribute to the OMB biases. As discussed in Section 3.2.2, these model errors will vary depending on the land surface (e.g., urban/rural) but are difficult to quantify.

4.3 | Vehicle-specific observation-minus-background departure distributions

Throughout the Met Office trial, 31 vehicles were used to produce vehicle-based observations. To investigate whether error statistics differ with vehicle, we plot OMB histograms for each of the 12 vehicles with the most observations between 09:00 and 17:00 in the QC-dataset in Figure 6. We use only observations between 09:00 and 17:00 so that the boundary layer is likely to be unstable
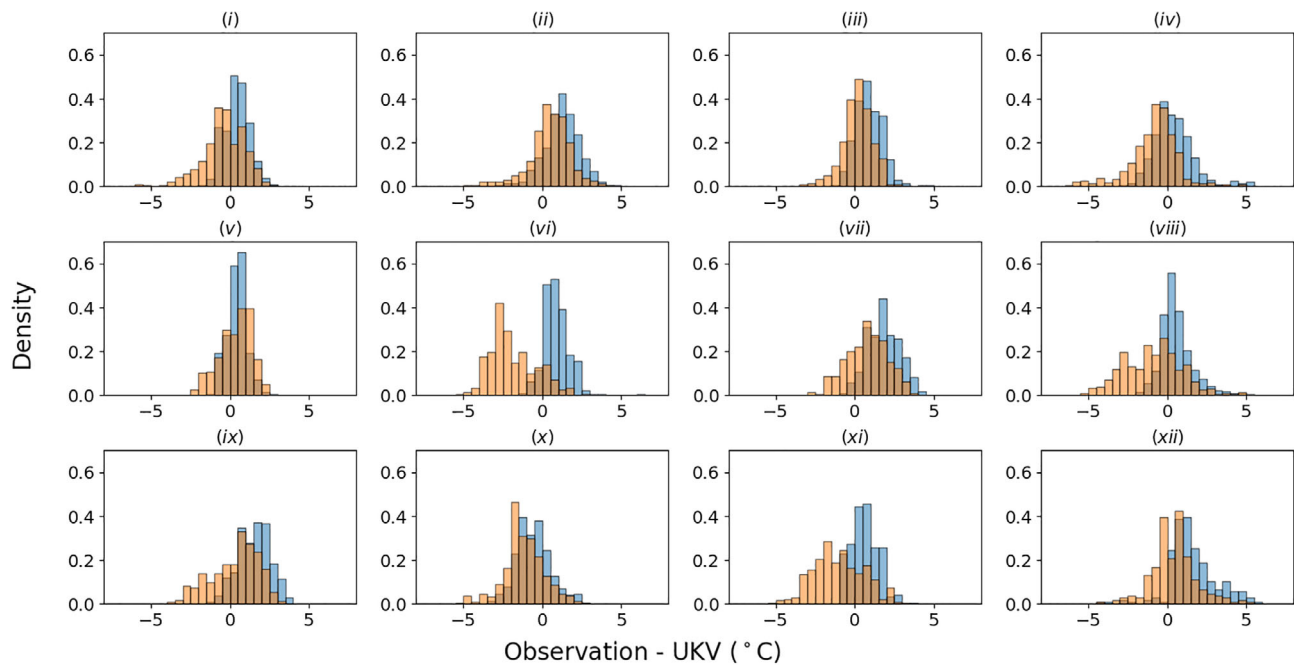
FIGURE 6 OMB histograms for the 12 vehicles with the most observations between 09:00 and 17:00 in the QC-dataset. The aOMB distributions are shown by the blue bins, the sOMB distributions are shown by the orange bins, and the overlap in distributions is shown by the composite. The same bins of width 0.5°C have been used for each histogram. Information on the statistics and observation meteorological conditions for each vehicle is given in Table 4.

TABLE 4 Summary of the OMB statistics for each vehicle in Figure 6. The uncertainty in the mean is at most 0.1°C for each vehicle OMB dataset. Also shown is the percentage of observations from a specific vehicle that appear in the weather-specific and seasonal datasets discussed in Section 4.2. Observations that do not appear in any of the weather-specific datasets are accounted for in the unclassified field on this table.

Summary statistics	Vehicle											
	(i)	(ii)	(iii)	(iv)	(v)	(vi)	(vii)	(viii)	(ix)	(x)	(xi)	(xii)
Number of observations	1533	1522	910	904	780	593	562	502	497	421	342	212
μ_a (°C)	0.4	1.2	0.9	0.4	0.4	0.9	1.8	0.6	1.5	−0.6	0.6	1.6
σ_a (°C)	0.9	1.1	0.9	1.1	0.8	0.9	1.0	1.0	1.0	1.0	0.9	1.2
μ_s (°C)	−0.4	0.4	0.1	−0.8	0.4	−1.9	0.8	−0.9	0.3	−1.2	−1.0	0.4
σ_s (°C)	1.2	1.2	1.0	1.3	1.0	1.2	1.2	1.4	1.2	1.1	1.3	1.2
Sunny percentage	0%	23%	22%	3%	34%	64%	13%	9%	36%	16%	22%	43%
Cloudy percentage	25%	23%	44%	18%	7%	10%	31%	26%	12%	47%	35%	38%
Rainy percentage	3%	10%	27%	20%	0%	0%	6%	11%	10%	6%	9%	0%
Unclassified percentage	72%	44%	7%	59%	59%	26%	54%	54%	42%	30%	34%	19%
Winter percentage	63%	41%	1%	47%	98%	10%	28%	47%	19%	47%	68%	0%
Spring percentage	37%	59%	99%	53%	2%	90%	72%	53%	81%	53%	32%	100%

(i.e., UKV surface-air temperature is greater than the 1.5m-air temperature). This is to avoid the complications of interpreting the OMB statistics experienced with the S2 time-series discussed in Section 4.1 and so that more observations can be classified into the weather-specific data

types discussed in Section 4.2. The OMB statistics are summarized in Table 4. Also included in Table 4 is the percentage of observations for each vehicle occurring in each weather-specific and seasonal dataset discussed in Section 4.2. We note that it is difficult to draw definitive

conclusions in this examination for two reasons. Firstly, many of the vehicles experience different weather conditions and there are many observations that we are unable to classify into a weather type. Secondly, there are only 12 vehicles with an acceptable number of observations that we can examine.

The majority of histograms shown in Figure 6 resemble normal distributions. The aOMB and sOMB distributions of vehicles (ii), (iii), (iv), (x), and (xii) are qualitatively similar with the visual distinction between them as a result of the difference in means. The remaining vehicles have noticeably different aOMB and sOMB distributions.

Examining the biases of the vehicle-specific OMB distributions shows that there are some vehicles that agree more with UKV 1.5m-air temperature than surface-air temperature as $|\mu_a| < |\mu_s|$. For these vehicles it is possible that the external air temperature sensor is located closer to 1.5 m height than the road surface or there are additional unknown factors affecting the vehicle-based observations as in S2 discussed in Section 4.1. The values of the biases μ_a and μ_s also vary substantially between vehicles. The sign of μ_s also varies with vehicle, whereas only vehicle (x) has negative μ_a, which suggests that some element of the vehicle's external air-temperature sensor or processing procedure may have a cold bias.

Except for vehicle (xii), we find that the aOMB dataset is less variable than the sOMB dataset (i.e., $\sigma_a < \sigma_s$) for all vehicles, which agrees with the results obtained in Sections 4.1 and 4.2. The values of the standard deviations σ_a and σ_s also vary substantially between vehicles. When stratifying the vehicles by seasonal contribution, we are able to find some agreement between the OMB dataset variability. This can be seen between the groups of vehicles (ii) and (vii), vehicles (iv), (viii), and (x), and vehicles (i) and (xi). Each vehicle in these groups contains similar ratios of winter to spring observations. For vehicles (iii), (vi), (ix), and (xii), which contain predominantly spring observations, we see that the aOMB standard deviation σ_a is similar except for vehicle (xii), and the sOMB standard deviation σ_s is similar except for vehicle (iii). This shows that vehicles may have similar OMB uncertainty if they have similar ratios of seasonal observations.

5 | CONCLUSION

In this work, we have examined a novel low-precision vehicle-based observation dataset obtained from a Met Office proof-of-concept trial. An overview of the quality control (QC) applied to the vehicle-based observations was given. The data that passed QC were examined and compared with UKV 1.5m-air-temperature and surface-

air-temperature model data, roadside weather information station (RWIS) data, and hourly MIDAS data. Using these datasets, we explored the characteristics of the vehicle-based observations that passed QC.

The QC procedure consisted of four tests that assessed different aspects of the vehicle-based observations. Reports that did not have an observation of air temperature or the necessary metadata to be tested were removed prior to the QC procedure. The climatological range test (CRT), stuck instrument test (SIT), and global positioning system (GPS) test were applied in parallel. Both the SIT and GPS test required vehicle identification, which may be unavailable in other crowdsourced and opportunistic datasets due to privacy concerns. While the majority of observations passed the CRT and SIT, a substantial number of observations were flagged by the GPS test due to unsuitable GPS update settings on the smartphone application and poor GPS signal. The observations that passed these three QC tests were put through a final sensor ventilation test (SVT) that flagged observations from vehicles driving below a predetermined sensor-ventilation-threshold speed. The SVT flagged a sizeable amount of data relative to the amount tested. The final quality-controlled dataset (QC-dataset) consisted of 25.6% of the observations obtained from the Met Office trial. Despite the high percentage of observations that failed QC, a large number of observations were obtained with a small number of participants in the Met Office trial. With more participants and the use of connected and autonomous vehicles, vehicle-based observations of air temperature have the potential to be the largest source of surface-based air-temperature data (Mahoney III & O'Sullivan, 2013). Use of vehicle-based observations in an operational setting would require an improved collection protocol to increase the percentage of observations that pass QC. Recommendations for future data collection and QC include correcting the smartphone application to record necessary metadata for all observations and reducing the requirements needed for the smartphone GPS update (Bell et al., 2021).

Using the QC-dataset, we investigated the uncertainty present in vehicle-based observations by analysing two OMB datasets. One dataset used UKV 1.5m-air temperature as the background (aOMB) and the other dataset used UKV surface-air temperature as the background (sOMB). Examining the OMB statistics of the QC-dataset, we found that the vehicle-based observations of air temperature were on average greater than the UKV model data and agreed more with surface-air temperature than 1.5m-air temperature. This is expected as the vehicle-based observations likely measure air temperature nearer to the surface than to a height of 1.5 m. However, there are several possible contributing factors to this result such as the quantization error, the difference in height between the vehicle-based observations and

the UKV grid box, or heat from the vehicle engine contaminating the vehicle-based observations. We also found that the sOMB uncertainty is greater than the aOMB uncertainty for the QC-dataset. This is likely because the UKV surface-energy balance has a much stronger influence on surface-air temperature than 1.5m-air temperature.

To examine how the vehicle-based observation uncertainty changes with weather conditions, we grouped the OMB datasets by sunny, cloudy, and rainy weather. For the sunny and cloudy OMB datasets, UKV surface-air temperature was on average greater than the vehicle-based observations, with the magnitude of the sOMB bias greatest for the sunny dataset when the vertical air-temperature gradient near the surface is large. However, as shown in an illustrative time-series example, vehicle-based observations can be in greater agreement with 1.5m-air temperature than surface-air temperature in sunny weather conditions. Possible explanations for this include the vehicle location (e.g., sea breeze effects) or the placement of the sensor used by the vehicle. For the rainy OMB dataset, when the vertical air-temperature gradient near the surface is small, we found that the vehicle-based observations were on average warmer than both UKV model fields. Inspecting the variability of the OMB datasets, we found that the sOMB variability is greatest in sunny weather conditions and smallest in rainy weather conditions. The aOMB variability was larger for the cloudy dataset than for the sunny dataset but still smallest for the rainy dataset. The large aOMB variability for the cloudy dataset may be due to changes in the sky-view factor caused by variable cloud cover or because it was the largest of the weather-specific datasets. These results strongly suggest that the uncertainty of vehicle-based observations of air temperature is weather-dependent. In particular, the uncertainty of vehicle-based observations will be largest in sunny weather conditions and smallest in rainy weather conditions.

To determine the effect of different vehicles on vehicle-based observations, the OMB datasets were grouped by vehicle. Due to the large number of observations with unclassified weather conditions and the different proportions of weather conditions experienced by vehicles, we were unable to distinguish between meteorological and vehicle effects on the vehicle-specific OMB distributions effectively. However, we note that vehicles with similar proportions of seasonal data may exhibit similar OMB variability. In order to determine the influence of the vehicle on the OMB statistics, further investigations into vehicle-based observations using a larger dataset must be conducted.

Vehicle-based observations are a potentially abundant source of low-cost, high-resolution meteorological information that can help improve the spatial coverage of surface-based observations (World Meteorological Organization, 2021a). Furthermore, vehicle-based observations and other crowdsourced datasets can provide information on microscale variations that MIDAS observations and other gridded datasets are unable to, such as urban heat islands (Chapman et al., 2017; Droste et al., 2017; Knight et al., 2010; Meier et al., 2017) and hailstorms (Clark et al., 2018). Improved understanding of microscale variations through high-resolution observational data is fundamental to the development of theory and numerical weather prediction (NWP) models with grid lengths of $\mathcal{O}(100)m$ (Barlow et al., 2017).

There are several issues regarding data collection and privacy in addition to the uncertainty characteristics, which must be addressed before vehicle-based observations may be utilized. We first note that an increase in precision of the vehicle-based observations will allow improved QC, understanding of the characteristics of the data, and value for NWP. Additionally, higher precision data will allow for improved exploration of vehicle-based observation characteristics and the observed meteorological dynamics (Mercelis et al., 2020). For QC, an alternative to vehicle identification must be used such that privacy concerns are mitigated. For assimilation, the uncertainty and bias associated with each observation must be sufficiently evaluated. This will require further trials to assess the effect of local meteorological conditions and the vehicle sensing instrument. Provided there are enough data in reasonable proximity in future studies, it would be useful to calculate and compare the sensible heat flux of the road and a convection-permitting NWP model surface. Despite these issues, vehicle-based observations are a promising opportunistic dataset for convection-permitting data assimilation.

thank two anonymous referees whose comments have helped improve the quality of this paper.

CONFLICT OF INTEREST

The authors declare that there is no conflict of interest.

AUTHOR CONTRIBUTIONS

Zackary Bell: Conceptualization (equal); data curation (lead); formal analysis (lead); investigation (equal); methodology (equal); software (lead); validation (lead); visualization (lead); writing – original draft (lead); writing – review and editing (equal). **Sarah Dance:** Conceptualization (equal); funding acquisition (lead); methodology (equal); project administration (equal); supervision (equal); writing – review and editing (equal). **Joanne Waller:** Conceptualization (equal); investigation (equal); methodology (equal); project administration (equal); supervision (equal); writing – review and editing (equal).

DATA AVAILABILITY STATEMENT

ORCID

Zackary Bell https://orcid.org/0000-0002-8427-1400
Sarah L. Dance https://orcid.org/0000-0003-1690-3338
Joanne A. Waller https://orcid.org/0000-0002-7783-6434

REFERENCES

Abdelhamid, S., Hassanein, H.S. & Takahara, G. (2014) Vehicle as a mobile sensor. *Procedia Computer Science*, 34, 286–295.

Anandakumar, K. (1999) A study on the partition of net radiation into heat fluxes on a dry asphalt surface. *Atmospheric Environment*, 33(24–25), 3911–3918.

Anderson, A.R., Chapman, M., Drobot, S.D., Tadesse, A., Lambi, B., Wiener, G. et al. (2012) Quality of mobile air temperature and atmospheric pressure observations from the 2010 development test environment experiment. *Journal of Applied Meteorology and Climatology*, 51(4), 691–701.

Barlow, J., Best, M., Bohnenstengel, S.I., Clark, P., Grimmond, S., Lean, H. et al. (2017) Developing a research strategy to better understand, observe, and simulate urban atmospheric processes at kilometer to subkilometer scales. *Bulletin of the American Meteorological Society*, 98(10), ES261–ES264.

Bell, S., Cornford, D. & Bastin, L. (2015) How good are citizen weather stations? Addressing a biased opinion. *Weather*, 70(3), 75–84.

Bell, Z., Dance, S.L. & Waller, J.A. (2020) Accounting for observation uncertainty and bias due to unresolved scales with the Schmidt-Kalman filter. *Tellus A: Dynamic Meteorology and Oceanography*, 72(1), 1–21.

Bell, Z., Dance, S.L., Waller, J.A. & O'Boyle, K. (2021) *Quality-control of vehicle-based temperature observations and future recommendations*. Forecasting research technical report 644. Exeter, Devon: Met Office.

BIPM, IEC, IFCC, ILAC, IUPAC, IUPAP, ISO & OIML. (2012) *International vocabulary of metrology - basic and general concepts and associated terms (VIM)*, Vol. 200, 3rd edition. Sèvres, Paris: JCGM, p. 2012.

Blair, G.S., Bassett, R., Bastin, L., Beevers, L., Borrajo, M.I., Brown, M. et al. (2021) The role of digital technologies in responding to the grand challenges of the natural environment: the Windermere Accord. *Patterns*, 2(1), 100156.

Boutle, I.A., Finnenkoetter, A., Lock, A. & Wells, H. (2016) The London Model: forecasting fog at 333 m resolution. *Quarterly Journal of the Royal Meteorological Society*, 142(694), 360–371.

Bremner, R. (2019) Ever-growing cars: why they keep on getting wider. *Autocar*. Available at: https://www.autocar.co.uk/car-news/features/investigation-why-are-cars-becoming-so-wide [Accessed 14th January 2021].

Buttell, R., Keer, L., Moles, M., Mansfield, A., Hanson, E. & Waring, P. (2020) *SWIS user guide v19*. Guildford, Surrey: Highways England.

Chapman, L. & Thornes, J.E. (2005) The influence of traffic on road surface temperatures: implications for thermal mapping studies. *Meteorological Applications*, 12(4), 371–380.

Chapman, L. & Thornes, J. (2011) What spatial resolution do we need for a route-based road weather decision support system? *Theoretical and Applied Climatology*, 104(3–4), 551–559.

Chapman, L., Bell, C. & Bell, S. (2017) Can the crowdsourcing data paradigm take atmospheric science to a new level? A case study of the urban heat island of London quantified using Netatmo weather stations. *International Journal of Climatology*, 37(9), 3597–3605.

Clark, p.A. (1998) The implementation and performance of a 1D model coupled to NWP forcing for low-cost site-specific forecasting. *AMS 2nd Urban Symposium, Albuquerque, New Mexico, Nov 1998*.

Clark, M.R., Webb, J.D. & Kirk, p.J. (2018) Fine-scale analysis of a severe hailstorm using crowd-sourced and conventional observations. *Meteorological Applications*, 25(3), 472–492.

Cosgrove, B.A., Lohmann, D., Mitchell, K.E., Houser, P.R., Wood, E.F., Schaake, J.C. et al. (2003) Real-time and retrospective forcing in the North American Land Data Assimilation System (NLDAS) project. *Journal of Geophysical Research-Atmospheres*, 108(D22), 8842.

Coulson, R., Evans, B. & Skea, A. (2012). Operational OpenRoad verification. *16th International Road Weather Conference, Helsinki, Finland, May 2012*.

Dance, S.L., Ballard, S.P., Bannister, R.N., Clark, P., Cloke, H.L., Darlington, T. et al. (2019) Improvements in forecasting intense rainfall: results from the FRANC (Forecasting Rainfall exploiting new data Assimilation techniques and Novel observations of Convection) project. *Atmosphere*, 10(3), 125.

Droste, A., Pape, J.-J., Overeem, A., Leijnse, H., Steeneveld, G.-J., Van Delden, A. et al. (2017) Crowdsourcing urban air temperatures through smartphone battery temperatures in São Paulo,

Brazil. *Journal of Atmospheric and Oceanic Technology*, 34(9), 1853–1866.

Dutra, E., Muñoz-Sabater, J., Boussetta, S., Komori, T., Hirahara, S. & Balsamo, G. (2020) Environmental lapse rate for high-resolution land surface downscaling: an application to ERA5. *Earth and Space Science*, 7(5), e2019EA000984.

Essery, R., Best, M., Betts, R., Cox, p.M. & Taylor, C.M. (2003) Explicit representation of subgrid heterogeneity in a GCM land surface scheme. *Journal of Hydrometeorology*, 4(3), 530–543.

FierceElectronics. (2014) *Temperature sensors to generate $8 billion revenue by 2020*. Available at: https://www.fierceelectronics.com/components/temperature-sensors-to-generate-8-billion-revenue-by-2020 [Accessed 8th January 2021].

Gustafsson, N., Janjić, T., Schraff, C., Leuenberger, D., Weissmann, M., Reich, H. et al. (2018) Survey of data assimilation methods for convective-scale numerical weather prediction at operational centres. *Quarterly Journal of the Royal Meteorological Society*, 144(713), 1218–1256.

Gustavsson, T., Bogren, J. & Green, C. (2001) Road climate in cities: a study of the Stockholm area, south-east Sweden. *Meteorological Applications*, 8(4), 481–489.

Harrison, G. (2015) *Meteorological measurements and instrumentation*, chapter 5. Hoboken, New Jersey: John Wiley & Sons, pp. 77–102.

Harrison, R.G. & Burt, S. (2020) Shall I compare thee to a summer's day? Art thou more temperate?... Sometimes too hot the eye of heaven shines. *Weather*, 75(6), 172–174.

Hertwig, D., Grimmond, S., Hendry, M.A., Saunders, B., Wang, Z., Jeoffrion, M. et al. (2020) Urban signals in high-resolution weather and climate simulations: role of urban land-surface characterisation. *Theoretical and Applied Climatology*, 142, 1–28.

Highways England. (2018) *Historical environmental sensor station data* Available at: https://www.swis.highwaysengland.co.uk/ [Accessed 30th April 2020].

Highways England. (2020) SWIS support. (Personal communication, 11th September 2020).

Hintz, K.S., O'Boyle, K., Dance, S.L., Al-Ali, S., Ansper, I., Blaauboer, D. et al. (2019a) Collecting and utilising crowdsourced data for numerical weather prediction: propositions from the meeting held in Copenhagen, 4–5 December, 2018. *Atmospheric Science Letters*, 20, e921.

Hintz, K.S., Vedel, H. & Kaas, E. (2019b) Collecting and processing of barometric data from smartphones for potential use in numerical weather prediction data assimilation. *Meteorological Applications*, 26(4), 733–746.

Hintz, K.S., Vedel, H., Kaas, E. & Nielsen, N. (2020) Estimation of wind speed and soughness length using smartphones: method and quality assessment. *Journal of Atmospheric and Oceanic Technology*, 37(8), 1319–1332.

Hintz, K.S., McNicholas, C., Randriamampianina, R., Williams, H.T., Macpherson, B., Mittermaier, M. et al. (2021) Crowdsourced observations for short-range numerical weather prediction: report from EWLAM/SRNWP meeting 2019. *Atmospheric Science Letters*, 22, e1031.

Hu, Y., Almkvist, E., Gustavsson, T. & Bogren, J. (2019) Modeling road surface temperature from air temperature and geographical parameters - implication for the application of floating car data in a road weather forecast model. *Journal of Applied Meteorology and Climatology*, 58(5), 1023–1038.

Janjić, T., Bormann, N., Bocquet, M., Carton, J., Cohn, S., Dance, S. et al. (2018) On the representation error in data assimilation. *Quarterly Journal of the Royal Meteorological Society*, 144(713), 1257–1278.

Karsisto, V. & Lovén, L. (2019) Verification of road surface temperature forecasts assimilating data from mobile sensors. *Weather and Forecasting*, 34(3), 539–558.

Kirk, p.J., Clark, M.R. & Creed, E. (2021) Weather observations website. *Weather*, 76(2), 47–49.

Knight, S., Smith, C. & Roberts, M. (2010) Mapping Manchester's urban heat island. *Weather*, 65(7), 188–193.

Lean, H.W., Clark, p.A., Dixon, M., Roberts, N.M., Fitch, A., Forbes, R. et al. (2008) Characteristics of high-resolution versions of the Met Office Unified Model for forecasting convection over the United Kingdom. *Monthly Weather Review*, 136(9), 3408–3424.

Madaus, L.E. & Mass, C.F. (2017) Evaluating smartphone pressure observations for mesoscale analyses and forecasts. *Weather and Forecasting*, 32(2), 511–531.

Mahoney, W.P., III & O'Sullivan, J.M. (2013) Realizing the potential of vehicle-based observations. *Bulletin of the American Meteorological Society*, 94(7), 1007–1018.

Meier, F., Fenner, D., Grassmann, T., Otto, M. & Scherer, D. (2017) Crowdsourcing air temperature from citizen weather stations for urban climate research. *Urban Climate*, 19, 170–191.

Mercelis, S., Watelet, S., Casteels, W., Bogaerts, T., van den Bergh, J., Reyniers, M. et al. (2020) Towards detection of road weather conditions using large-scale vehicle fleets. *2020 IEEE 91st Vehicular Technology Conference (VTC2020-Spring)*, IEEE, 1–7.

Mercelis, S., Watelet, S. & Casteels, W. (2021) Personal communication, 3rd March 2021.

Met Office. (2006) *MIDAS: UK daily temperature data. Data retrieved from online CEDA archive*, NCAS British Atmospheric Data Centre. Available at: https://catalogue.ceda.ac.uk/uuid/220a65615218d5c9cc9e4785a3234bd0 [Accessed 16th June 2019].

Met Office (2016) NWP-UKV: Met Office UK Atmospheric High Resolution Model data. Data retrieved from online CEDA archive, NCAS British Atmospheric Data Centre. Available at: https://catalogue.ceda.ac.uk/uuid/f47bc62786394626b665e23b658d385f [Accessed 16th June 2019].

Met Office. (2018) *Daily weather summary*. Available at: https://www.metoffice.gov.uk/research/library-and-archive/publications/daily-weather-summary [Accessed 15th May 2020].

Milan, M., Macpherson, B., Tubbs, R., Dow, G., Inverarity, G., Mittermaier, M. et al. (2020) Hourly 4D-Var in the Met Office UKV operational forecast model. *Quarterly Journal of the Royal Meteorological Society*, 146(728), 1281–1301.

Mirza, A.K., Ballard, S.P., Dance, S.L., Maisey, P., Rooney, G.G. & Stone, E.K. (2016) Comparison of aircraft-derived observations with in situ research aircraft measurements. *Quarterly Journal of the Royal Meteorological Society*, 142(701), 2949–2967.

Muller, C., Chapman, L., Johnston, S., Kidd, C., Illingworth, S., Foody, G. et al. (2015) Crowdsourcing for climate and atmospheric sciences: current status and future potential. *International Journal of Climatology*, 35(11), 3185–3203.

Nipen, T.N., Seierstad, I.A., Lussana, C., Kristiansen, J. & Hov, Ø. (2020) Adopting citizen observations in operational weather

prediction. *Bulletin of the American Meteorological Society*, 101(1), E43–E57.

Oke, T.R., Mills, G., Christen, A. & Voogt, J.A. (2017) *Urban climates*, chapter 6. Cambridge, England: Cambridge University Press, pp. 156–196.

Overeem, A., Robinson, J.R., Leijnse, H., Steeneveld, G.-J.P., Horn, B. & Uijlenhoet, R. (2013) Crowdsourcing urban air temperatures from smartphone battery temperatures. *Geophysical Research Letters*, 40(15), 4081–4085.

Padarthy, M. & Heyns, E. (2019) Identification and classification of slippery winter road conditions using commonly available vehicle variables. *Transportation Research Record*, 2673(2), 60–70.

Porson, A., Clark, p.A., Harman, I., Best, M. & Belcher, S. (2010) Implementation of a new urban energy budget scheme in the MetUM. Part I: description and idealized simulations. *Quarterly Journal of the Royal Meteorological Society*, 136(651), 1514–1529.

Prusa, J.M., Segal, M., Temeyer, B.R., Gallus, W.A., Jr. & Takle, E.S. (2002) Conceptual and scaling evaluation of vehicle traffic thermal effects on snow/ice-covered roads. *Journal of Applied Meteorology*, 41(12), 1225–1240.

Siems-Anderson, A.R., Walker, C.L., Wiener, G., Mahoney, W.P., III & Haupt, S.E. (2019) An adaptive big data weather system for surface transportation. *Transportation Research Interdisciplinary Perspectives*, 3, 100071.

Siems-Anderson, A.S., Lee, J.A., Brown, B., Wiener, G. & Linden, S. (2020) Impacts of assimilating observations from connected vehicles into a numerical weather prediction model. *Transportation Research Interdisciplinary Perspectives*, 8, 100253.

Steeneveld, G.-J., Koopmans, S., Heusinkveld, B., Van Hove, L. & Holtslag, A. (2011) Quantifying urban heat island effects and human comfort for cities of variable size and urban morphology in the Netherlands. *Journal of Geophysical Research-Atmospheres*, 116(D20), D20129.

Stull, R.B. (1988a) *An introduction to boundary layer meteorology*, chapter 1. Berlin/Heidelberg, Germany: Springer Science & Business Media, pp. 9–19.

Stull, R.B. (1988b) *An introduction to boundary layer meteorology.*, chapter 12. Berlin/Heidelberg, Germany: Springer Science & Business Media, pp. 499–542.

Sun, J., Xue, M., Wilson, J.W., Zawadzki, I., Ballard, S.P., Onvlee-Hooimeyer, J. et al. (2014) Use of NWP for nowcasting convective precipitation: recent progress and challenges. *Bulletin of the American Meteorological Society*, 95(3), 409–426.

Tchir, J. (2016) Why the car thermometer isn't affected by engine heat or wind. *The Globe and Mail*. Available at: https://www.theglobeandmail.com/globe-drive/culture/commuting/why-the-car-thermometer-isnt-affected-by-engine-heat-or-wind/article28765614/ [Accessed 16th June 2019].

Verheul, E., Hicks, C. & Garcia, F.D. (2019) IFAL: issue first activate later certificates for V2X. *2019 IEEE European Symposium on Security and Privacy (EuroS P)*, 279–293.

Waller, J.A. (2020) Editorial: the use of unconventional observations in numerical weather prediction. *Meteorological Applications*, 27(5), e1948.

Waller, J.A., Dance, S.L. & Lean, H.W. (2021) Evaluating errors due to unresolved scales in convection perimitting numerical weather prediction. *Quarterly Journal of the Royal Meteorological Society*, 147, 2657–2669.

Warren, E., Charlton-Perez, C., Kotthaus, S., Lean, H., Ballard, S., Hopkin, E. et al. (2018) Evaluation of forward-modelled attenuated backscatter using an urban ceilometer network in London under clear-sky conditions. *Atmospheric Environment*, 191, 532–547.

Widrow, B., Kollar, I. & Liu, M.-C. (1996) Statistical theory of quantization. *IEEE Transactions on Instrumentation and Measurement*, 45(2), 353–361.

Wolters, D. & Brandsma, T. (2012) Estimating the urban heat island in residential areas in the Netherlands using observations by weather amateurs. *Journal of Applied Meteorology and Climatology*, 51(4), 711–721.

World Meteorological Organization. (2021a) *Observing systems capability analysis and review tool (OSCAR)*. Available at: https://space.oscar.wmo.int [Accessed 26th September 2021].

World Meteorological Organization. (2021b) *Variable: Air pressure (near surface)*. Available at: https://space.oscar.wmo.int/variables/view/air_pressure_near_surface [Accessed 8th August 2021].

Zahumenskỳ, I. (2004) *Guidelines on quality control procedures for data from automatic weather stations*. Geneva: World Meteorological Organization.